Permeability of continental crust influenced by internal and external forcing

S. A. ROJSTACZER[1], S. E. INGEBRITSEN[2] AND D. O. HAYBA[3]

[1]*Palo Alto, CA;* [2]*U.S. Geological Survey, Menlo Park, CA;* [3]*U.S. Geological Survey, Reston, VA, USA*

ABSTRACT

The permeability of continental crust is so highly variable that it is often considered to defy systematic characterization. However, despite this variability, some order has been gleaned from globally compiled data. What accounts for the apparent coherence of mean permeability in the continental crust (and permeability–depth relations) on a very large scale? Here we argue that large-scale crustal permeability adjusts to accommodate rates of internal and external forcing. In the deeper crust, internal forcing – fluxes induced by metamorphism, magmatism, and mantle degassing – is dominant, whereas in the shallow crust, external forcing – the vigor of the hydrologic cycle – is a primary control. Crustal petrologists have long recognized the likelihood of a causal relation between fluid flux and permeability in the deep, ductile crust, where fluid pressures are typically near-lithostatic. It is less obvious that such a relation should pertain in the relatively cool, brittle upper crust, where near-hydrostatic fluid pressures are the norm. We use first-order calculations and numerical modeling to explore the hypothesis that upper-crustal permeability is influenced by the magnitude of external fluid sources, much as lower-crustal permeability is influenced by the magnitude of internal fluid sources. We compare model-generated permeability structures with various observations of crustal permeability.

Key words: geothermal, groundwater, metamorphic, numerical modeling, permeability

Received 25 January 2008; accepted 17 April 2008

Corresponding author: Steven Ingebritsen, U.S. Geological Survey, Menlo Park, CA, USA.
Email: seingebr@usgs.gov. Tel: +1 650 329 4422. Fax: +1 650 329 4463.

INTRODUCTION

Permeability (k) is a measure of the relative ease of fluid flow under unequal pressure. The permeability of the Earth's crust is of great interest because it largely determines the feasibility of advective solute transport (requiring $k > \sim 10^{-20}$ m^2 under normal crustal conditions), advective heat transport (requiring $k \geq \sim 10^{-16}$ m^2), and the generation of elevated fluid pressures by processes such as physical compaction, heating, and mineral dehydration (requiring $k \leq \sim 10^{-17}$ m^2 over length scales of 100s of meters) (Fig. 1).

The permeability of the shallow continental crust is so highly variable that it is often considered to defy systematic characterization. The measured permeability of common geologic media varies by approximately 16 orders of magnitude, from values as low as 10^{-23} m^2 in intact crystalline rock, intact shales, and fault gouge, to values as high as 10^{-7} m^2 in well-sorted gravels. In the upper crust, permeability exhibits extreme heterogeneity, both among geologic units and within particular units. Field-based measurements of layered ash-flow tuff show up to 10^4-fold variation between welded and unwelded zones (e.g. Winograd, 1971). Similarly large variations have been measured within single soil units (Mitchell, 1993). Even larger variations in *in situ* permeability have been inferred between basalts near the surface of Kilauea volcano ($k \sim 10^{-10}$ to 10^{-9} m^2) and compositionally identical rocks at 1- to 2-km depth ($k \sim 10^{-16}$ to 10^{-15} m^2) (Ingebritsen and Scholl, 1993).

Despite this extreme variability, some order has been revealed in globally compiled data. In the early 1980s it was proposed, based on compilations of *in situ* hydraulic test data, that the mean *in situ* permeability of crystalline rocks in the uppermost crust (<1 km depth) is approximately 10^{-14} m^2 (Brace, 1980). This result for the very shallow crust is borne out by more recent *in situ* data (Hsieh, 1998), whereas other *in situ* data suggest an identifiable decrease in permeability with depth (Clauser, 1992).
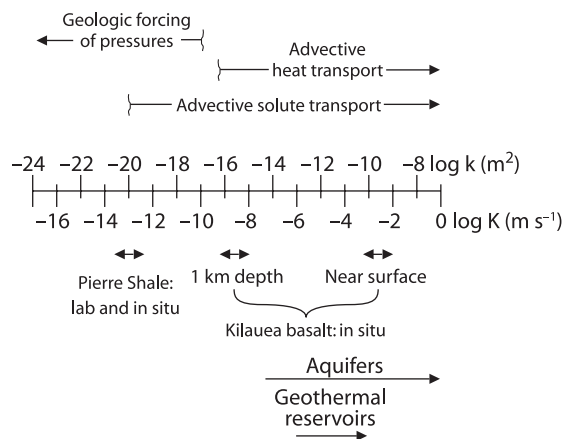
Fig. 1. Range of permeabilities observed in geologic media, showing certain process-limiting values and other selected values. Hydraulic conductivity ($K = k\rho_f g/\mu$, m s^{-1}) is for water density ρ_w and viscosity μ_w at 15°C. From Ingebritsen et al. (2006).

Direct *in situ* measurements of permeability are rare below depths of 2–3 km and nonexistent below 10 km depth. As an alternative, geothermal data and estimates of fluid flux during prograde metamorphism have been used to constrain the permeability of tectonically active portions of the continental crust (Manning and Ingebritsen, 1999). A power-law fit to these data yields log $k = -14 - 3.2$ log z, where k is in meters squared (m^2) and z is depth in kilometers. This permeability–depth relation for the deeper crust has since been shown to be reasonably compatible with independently compiled data (Townend and Zoback, 2000; Shmonov et al., 2003; Saar and Manga, 2004; Stober and Bucher, 2007).

What accounts for the apparent coherence of mean permeability in the continental crust (and permeability–depth relations) on a very large scale? Here we argue that large-scale crustal permeability adjusts to accommodate rates of internal and external forcing. In the deeper crust, internal forcing – fluxes primarily induced by metamorphism and mantle degassing – is dominant, whereas in the shallow crust, external forcing – the vigor of the hydrologic cycle – is a primary control.

CRUSTAL PERMEABILITY AS A DYNAMIC PARAMETER

A petrologic view of the deep crust is that permeability represents a dynamic response to dewatering and fluid production (e.g. Hanson, 1992; 1995; 1997; Yardley and Baumgartner, 2007). This view is in stark contrast to the standard hydrogeologic concept of permeability as a material property that exerts control on fluid flow. In fact, scientists concerned mainly with relatively hot, high-pressure conditions in the deeper crust have suggested that the parameter called 'intrinsic permeability' by hydrogeologists

should instead be named 'dynamic permeability' (Cathles and Adams, 2005).

The permeability of the deep, tectonically active crust can reasonably be viewed as a dynamic response to metamorphic and magmatic devolatilization. Analyses of metamorphic phase equilibria and fluid-inclusion data indicate that fluid pressure is close to the lithostatic load during prograde metamorphism (e.g. Fyfe et al., 1978). Sufficiently overpressured fluids cannot be contained in the crust and create the permeability necessary to escape. Metamorphic fluid fluxes and inferred permeabilities during metamorphism (cf. Manning and Ingebritsen, 1999), are likely controlled by dewatering rates of metamorphic piles. These fluids and other 'endogenic' (Crossey et al., 2006) fluids can be transmitted to the upper crust where they mix with meteoric fluids (cf. Ingebritsen and Manning, 1999, 2002). Metamorphic and other non-meteoric fluids have been identified in a variety of orogenic belts on the basis of diverse lines of evidence, including helium, carbon, and strontium isotopes (e.g. Barnes, 1970; Barnes et al., 1984; Kamensky et al., 1990; Dahlgren et al., 1993; Oliver et al., 1993; Dunai and Touret, 1993; James et al., 1999; Newell et al., 2005; Crossey et al., 2006; Kennedy and van Soest, 2007).

In the deep, hot crust, under a suprahydrostatic fluid-pressure regime, a causal relation between fluid flux and permeability seems quite plausible (cf. Yardley, 1986; Hanson, 1995, 1997; Sibson, 1996; Connolly, 1997; Cathles and Adams, 2005). It is not obvious that such a relation should pertain in the relatively cool, brittle upper crust, where near-hydrostatic fluid pressures are the norm in crystalline rocks (cf. Huenges et al., 1997; Zoback and Zoback, 1997, Townend and Zoback, 2000). In this paper, we use first-order calculations and numerical modeling to explore the hypothesis that upper-crustal permeability is influenced by the magnitude of external fluid sources, much as lower-crustal permeability is influenced by the magnitude of internal fluid sources.

As a first step, we show that the gross hydrogeologic characteristics of the western United States (roughly west of the 100th meridian) are compatible with the mean recharge rate if the water table is a subdued replica of the topography (Fig. 2). We solve the Dupuit-Forcheimer equation in two dimensions to determine the permeability required for a 'subdued topography' water table, defining 'subdued topography' as half of the regional slope. The length of the groundwater flow path, the slope of the land surface (a surrogate for the slope of the water table), and the groundwater recharge rate are the critical parameters constraining permeability (Fig. 3). We infer flow-path length from estimates of drainage density in basins (Moglen et al., 1998) and scaling relations from high-order basins (Rodriguez-Iturbe and Rinaldo, 1997), assuming a fifth-order basin for
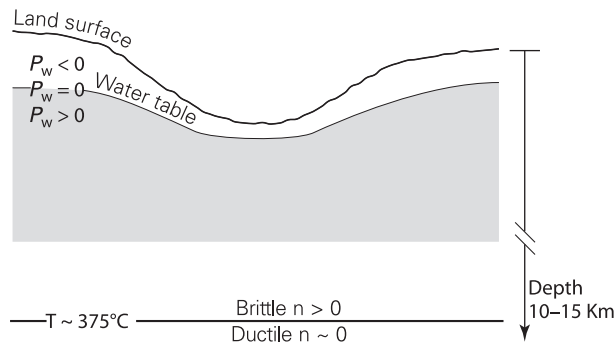
Fig. 2. Schematic diagram of a hydrogeologic system showing the domain of interest between the water table and the brittle–ductile transition. The water table is defined as the surface where pressure in the liquid phase, P_w, is equivalent to atmospheric pressure, P_{atm}. Below the water table $P_w > P_{atm}$ and above the water table $P_w < P_{atm}$, because air and water coexist in the pore space). The brittle–ductile transition occurs at 10–15 km depth in typical crustal rocks along regional metamorphic geotherms. Below the brittle–ductile transition, ductile deformation presumably collapses porosity ($n \sim 0.0$), unless fluid pressure is close to the lithostatic load.
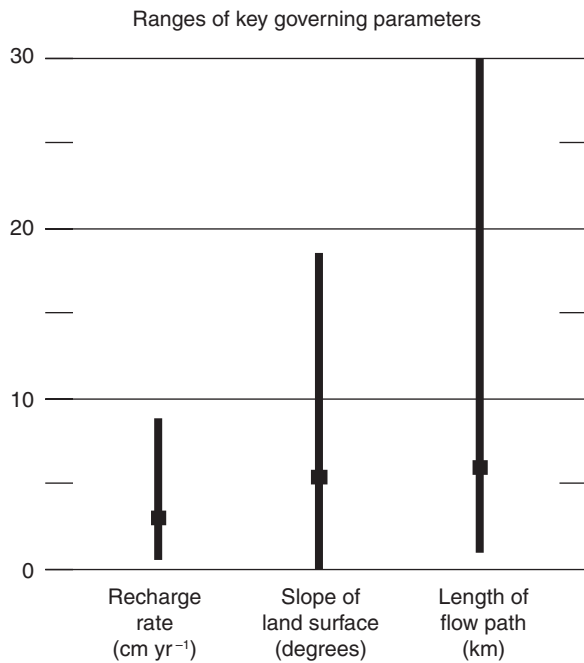

Fig. 3. Key constraints governing the permeability of the uppermost crust, with estimated 95% confidence intervals. Data represent conditions in the United States west of the 100th meridian. Recharge rate is estimated for 1994, a sub-median water year.

Fig. 4. Permeability required to maintain a water table that is a subdued replica of the topography in a homogeneous crust, as a function of recharge rate and slope of the water table. Permeabilities were determined by solution of the Dupuit-Forchheimer equation for fluid flow in unconfined aquifers with the modification that, in basin-wide flow, roughly half of the recharge is lost to lower-order streams (Toth, 1963). Dashed lines denote mean permeability of the uppermost crystalline crust (Brace, 1980) and mean slope of the western United States.

groundwater flow. We determine slope from 1-km digital elevation models (Wolock and McCabe, 2000). Recharge is based on data from the entire U.S. Geological Survey stream-gauging network for the State of California, and determined by dividing the magnitude of summer 1994 bas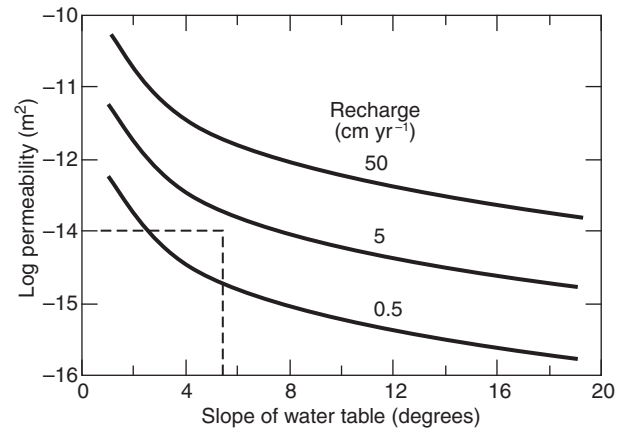eflow by the area of each drainage basin. Streams with significant human influences are excluded, and where baseflow is zero a recharge rate of 0.5 cm year^{-1} is assumed, based on data from the vicinity of Yucca Mountain, Nevada (Flint *et al.*, 2002).

Regional flow typically entails nested flow paths at a variety of scales as in Toth's (1963) iconic plot. To account for this effect we assume that, in basin-wide flow, roughly half of the recharge is lost to lower-order streams (Toth, 1963). For a mean western United States slope (5.5°) and recharge rate (3 cm year^{-1} or 10^{-9} m s^{-1}), the permeability required to produce a water table that is a subdued replica of topography is 10^{-14} m[2] (Fig. 4).

The optimum permeability required to support a 'subdued topography' water table in the western United States is thus identical to the mean *in situ* permeability of crystalline rocks in the uppermost crust (Brace, 1980). There is a growing body of evidence that upper-crustal permeability may be affected both by small variations in fluid pressure and small strains in the Earth. If this is the case, the compatibility between mean permeability and mean recharge implies that recharge can control the magnitude of permeability in the shallow crust.

Some of the clearest evidence for fluid-pressure-induced rock failure at relatively low fluid pressures comes from seismicity induced by fluid injection. For instance, fluid injection-induced failure at depths ≥3.6 km at the Rocky Mountain Arsenal, Colorado, appears to have occurred at fluid pressures that were subhydrostatic relative to the land surface ($P_{failure} \sim 30$ MPa; $dP/dz \sim 8$ MPa/km, or ~80% of hydrostatic) (Hsieh and Bredehoeft, 1981). The pressure increase required to trigger failure at the Rocky

Mountain Arsenal was approximately 3.2 MPa, which amounts to a pressure increment of approximately 9% relative to a hydrostat calculated from the land surface or approximately 12% relative to the estimated pre-injection pressure in the injection zone ($\sim$27 MPa). At the Soultz, France, hot-dry-rock site, differential pressures 15–20% above hydrostatic caused a 200-fold increase in the transmissivity of an injection zone at roughly 3 km depth (Evans *et al.*, 2005).

Seasonal variations in seismicity, documented at a growing number of sites worldwide, imply that rock failure can actually be induced by small, seasonal hydrologic changes (Wolf *et al.*, 1997; Ohtake and Nakahara, 1999; Heki, 2003; Saar and Manga, 2003; Christiansen *et al.*, 2005, 2007; Hainzl *et al.*, 2006; Bollinger *et al.*, 2007; Bettinelli *et al.*, 2008). At many of these localities, changes in water-table elevation appear to represent the largest seasonal forcing, ranging from 1–20 m (10–200 kPa) at the land surface to approximately 1–120 kPa at seismogenic depths of 2–8 km (Christiansen *et al.*, 2005). These analyses of seasonal seismicity imply that the fluid-pressure increase required for rock failure may be exceedingly small, amounting to <1% of the hydrostatic pressure at seismogenic depths. Certain observations of reservoir-induced seismicity also imply very low failure thresholds (see, e.g. the recent and thorough compilation by Talwani *et al.,* 2007).

Based on these various lines of evidence, it is reasonable to infer that permeability in the brittle upper crust may be affected by rock failure or fracture slip at near-hydrostatic fluid pressures (e.g. Hsieh and Bredehoeft, 1981) triggered by very small changes in fluid pressure (e.g. Christiansen *et al.*, 2005). Moreover, data from a number of deep (to 2.5 km) drill holes in the western United States indicate that most hydraulically conductive fractures are critically stressed (Barton *et al.*, 1995; Townend and Zoback, 2000); only those fractures oriented such that they are near-failure under the current stress regime tend to be hydraulically conductive. This implies that a small increase in fluid pressure can bring additional, appropriately oriented fractures to a state of failure.

Recent studies confirm that in the absence of active fracturing, permeability should tend to decrease with time (Elkhoury *et al.*, 2006; Claesson *et al.*, 2007; Claesson, 2007). In the California Coast Ranges, the response of water levels in very shallow (<250 m) wells to solid-Earth tides was used to measure permeability over a 20-year period (Elkhoury *et al.*, 2006). Permeability increased by as much as a factor of 3 coincident with seven distant (10–200 km) earthquakes during this period, with the magnitude of increase proportional to the peak ground velocity at the site. Between earthquakes, permeability decayed steadily towards background values of 1×10^{-15} m^2 (for one of the two monitored wells) and 6×10^{-15} m^2 (for

the other well). Post-earthquake fracture sealing and permeability reduction over similar time scales of years to decades have been inferred from geochemical observations in wells in northern Iceland (Claesson *et al.*, 2007) and northeastern India (Claesson, 2007).

Thus our conceptual model assumes that, in tectonically active regions, the state of stress for many fractures – enough to provide a percolating network – is in a state of incipient failure. In the absence of active fracturing driven by tectonics and fluid transport, permeability tends to decrease, as mineral precipitation and hydrothermal alteration seal fractures and pores and cause the fracture network to become disconnected. The average permeability of the crust at any particular time results from a competition between cracking and healing.

NUMERICAL SIMULATION OF PERMEABILITY EVOLUTION

We use numerical simulation to further explore the hypothesis that the mean large-scale permeability of tectonically active continental crust is influenced by external (meteoric recharge) and internal (metamorphic and magmatic) forcing. We devise a set of numerical simulations in which crustal permeability is, effectively, the primary dependent variable. Other variables are estimated independently on the basis of best-available independent evidence.

We employ the U.S. Geological Survey's HYDRO-THERM model, which simulates three-dimensional, multi-phase flow of pure water over the temperature range of 0–1200°C. The published version of HYDROTHERM allows intrinsic permeability (k_x, k_y, k_z) to vary arbitrarily in space and also as a function of temperature (T) (Hayba and Ingebritsen, 1994). We have added the capability to vary k according to user-designated functions of fluid pressure (P) and time (t), so that permeability can now be treated as $k(x, y, z, T, P, t)$. For example, when P reaches a designated threshold, k_x, k_y, and k_z increase by designated amounts. The underlying assumption is that in any volume of fractured rock there is some appropriately oriented fracture that will slip if P increases sufficiently. The decrease of permeability with time represents processes such as hydro-thermal alteration and diagenesis and can be described by a variety of user-designated functions.

Governing equations

HYDROTHERM simulates multiphase, multidimensional fluid flow and heat transport by solving mass- and energy-balance equations that are posed in terms of pressure (P) and enthalpy (H), respectively. Our simulations entail single-phase conditions, so that the governing equations effectively reduce to:

$$\frac{\partial(n\rho_\text{w})}{\partial t} - \nabla \cdot \left[\frac{\rho_\text{w}\bar{k}}{\mu_\text{w}} (\nabla P + \rho_\text{w} \mathcal{g} \nabla z) \right] - R_\text{m} = 0 \qquad (1)$$

and

$$\frac{\partial[n\rho_\text{w}H_\text{w} + (1-n)\rho_\text{r}H_\text{r}]}{\partial t} - \nabla \cdot \left[\frac{\rho_\text{w}\bar{k}H_\text{w}}{\mu_\text{w}} (\nabla P + \rho_\text{w}\mathcal{g}\nabla z) \right]$$
$$- \nabla \cdot K_\text{m}\nabla T - R_\text{h} = 0, \qquad (2)$$

where the vector operator ∇ indicates $\mathbf{i}\partial/\partial x + \mathbf{j}\partial/\partial y + \mathbf{k}\partial/\partial z$, the overbar indicates that $\bar{k}$ is a second-rank tensor in the general case, n is porosity, ρ is density, t is time, k is permeability, μ is viscosity, $\mathcal{g}$ is gravitational acceleration, R represents a source or sink, K_m is the bulk thermal conductivity, and the subscripts 'w' and 'r' refer to liquid water and rock, respectively. Assumptions inherent in these governing equations are discussed in detail elsewhere (Faust and Mercer 1979; Hayba and Ingebritsen, 1994).

The capability of HYDROTHERM to accurately represent the physical properties of water is essential to our analysis. We anticipate pressures of up to approximately 100 MPa and temperatures in excess of 300°C in the simulation domain, so that water density ρ_w varies by about 30% and water viscosity μ_w by a factor of 15–20 within the domain. Because the fluid volume flux is governed by hydraulic conductivity ($k\rho_\text{w}\mathcal{g}/\mu_\text{w}$), and we are interested only in permeability (k), it is essential to represent ρ_w and μ_w accurately. HYDROTHERM uses a lookup table interrogated by a bicubic interpolation routine to accurately represent fluid properties over a pressure range of 0.05–1000 MPa and 0–1200°C.

Geometry

We simulate fluid flow and heat transport in a two-dimensional vertical section (Fig. 5). The depth of the section
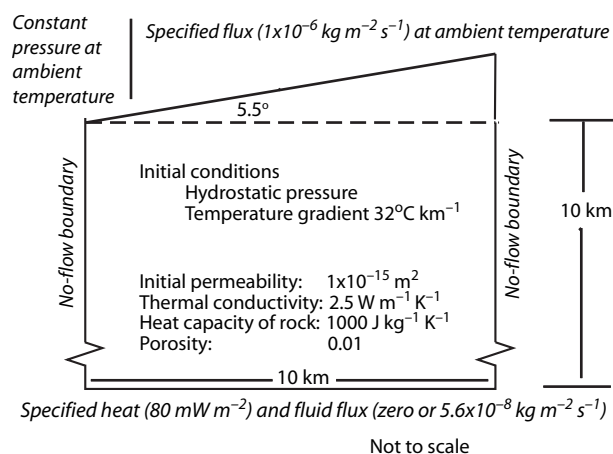

Fig. 5. Geometric model used in numerical simulations. See text for discussion of boundary conditions, initial conditions and selected parameters.

along the left-hand boundary is 10 km, encompassing the domain of interest between the water table and the brittle–ductile transition (Fig. 2). This transition occurs at 10–15 km depth in typical crustal rocks along regional metamorphic geotherms. The length of the section is also 10 km, slightly longer than the mean western United States flow path estimated previously (Fig. 3). The land-surface slope is assigned the mean western United States value of 5.5°. The space–discretization is coarse in the x-direction ($\Delta x = 1.0$ km) and finer in the z-direction ($\Delta z = 0.1$ km).

Boundary and initial conditions

Boundary and initial conditions are assigned as follows (Fig. 5). The upper boundary is divided into two portions, a small (one node) lower-elevation segment and the remaining upper-elevation portion. This upper portion is assigned the mean western United States recharge rate of 3 cm year^{-1} (Fig. 3; 10^{-9} m s^{-1} or 1×10^{-6} kg m^{-2} s^{-1}) at ambient temperature. We accomplish this by adding a source flux directly beneath the surface nodes, which are assigned a relatively low permeability (log $k = -16$) at constant pressure and temperature. This approach allows the pressure and permeability to vary in all nodes except at those nodes right at the surface, without having the surface flux immediately exit the model domain. Most (approximately 85%) of the fluids exit the domain at the lower-elevation segment of the upper boundary, which is a constant pressure–enthalpy boundary at atmospheric pressure and ambient temperature with a permeability of 1×10^{-12}. Ambient temperature along the upper boundary is 5°C at the highest land-surface elevation and increases by 5.5°C per kilometer of elevation loss (the adiabatic lapse rate). The lower boundary is assigned a heat flux of 80 mW m^{-2}, representative of regions of Neogene tectonism and magmatism (Sclater *et al.*, 1980), and a fluid flux of either zero (no flux) or 5.6×10^{-8} kg m^{-2} s^{-1}, which is the arithmetic mean of a global compilation of metamorphic flux data (Manning and Ingebritsen, 1999). The lateral boundaries are closed and insulated, under the assumption of symmetry.

We implicitly assume constant-stress boundary conditions such that the only changes in effective stress are related to changes in fluid pressure. We further assume that within any volume of fractured rock there is an appropriately oriented fracture that will slip if pressure increases significantly above an equilibrium state. The latter assumption is reasonable for the western United States where the rocks are critically stressed (Townend and Zoback, 2000). The failure under subhydrostatic conditions at the Rocky Mountain Arsenal (Hsieh and Bredehoeft, 1981) is good evidence that the equilibrium state may involve near-hydrostatic pressures.

The upper (water-table) boundary of the model poses the most problematic boundary condition, both conceptually and computationally. In nature, water-table position would adjust to accommodate (for instance) variations in meteoric recharge. However, in the version of HYDRO-THERM that we employ, the upper boundary is fixed in space. Thus simulated pressure fluctuations just below the upper boundary (Fig. 6) serve as a proxy for water-table movement. In the simulations discussed below, the magnitude of simulated pressure fluctuations near the upper boundary is comparable with that typically associated with water-table excursions in nature (Fig. 6: ΔP near the upper boundary generally $<\pm 0.3$ MPa, decaying with depth).

The initial pressure conditions are hydrostatic, consistent with observations to nearly 10 km depth in crystalline continental crust (Huenges et al., 1997; Zoback and Zoback, 1997). Bulk thermal conductivity (K_m in Eqn. 2) and specific heat of rock (H_r) are assigned typical upper-crustal values of 2.5 W m^{-1} K^{-1} and 1000 J kg^{-1} K^{-1}, respectively, and porosity is assigned an arbitrary value of 0.01 (Fig. 5). The initial temperature gradient is uniform at 32°C km^{-1}, representing conduction-only conditions for a basal heat flux of 80 mW m^{-2} and a uniform thermal conductivity of 2.5 W m^{-1} K^{-1}.

Transient behavior

We have not attempted to explicitly model either the complex physics of fracturing (e.g. Marder and Fineberg, 1996; Scholz, 2002) or the geochemical processes responsible for permeability loss. Instead, we invoke simple rules that are consistent with field observations: (i) that fluid pressures are near-hydrostatic (i.e. generally ≤110% of hydrostatic) in the crystalline crust (Huenges et al., 1997;

Zoback and Zoback, 1997); (ii) that failure (and presumably k increase) occurs in response to relatively small pressure increases (Hsieh and Bredehoeft, 1981; Rojstaczer and Bredehoeft, 1988); (iii) that fractured-rock permeability decays quite rapidly over time (e.g. Elkhoury et al., 2006); and (iv) that the crust has sufficient permeability to accommodate representative fluxes – meteoric recharge and endogeneous fluids – under near-hydrostatic conditions.

In our base-case simulation, permeability starts to increase at a pressure threshold of 105% of hydrostatic and increases at a maximum rate (doubling time 0.05 years) when pressure exceeds 115% of hydrostatic. We assume that permeability loss results from mineral precipitation and alteration, so that permeability will decay with time as some function of fluid flux. To simplify the calculation, we use permeability as a proxy for fluid flux and use a log-linear function to scale permeability loss with time. The maximum decrease in permeability is 10% per year at $k = 10^{-12}$ m^2, which is the maximum permeability we consider in these experiments. Although somewhat faster decay rates have been inferred in both shallow-groundwater (Elkhoury et al., 2006) and high-temperature environments (Moore et al., 1983; Lowell et al., 1993; Claesson et al., 2007), we assume that substantial loss of permeability typically requires decades to centuries. We assume that fluid flux and therefore permeability loss are negligible for $k \leq 10^{-19}$ m^2. The effects of various other functional descriptions of permeability creation and decay are explored elsewhere (D.O. Hayba and S.E. Ingebritsen, unpublished observations).

Simulations with pressure- and time-dependent permeability cannot reach a true steady state but instead show continuous variation, because of the competition between failure and permeability decay. Simulated permeability
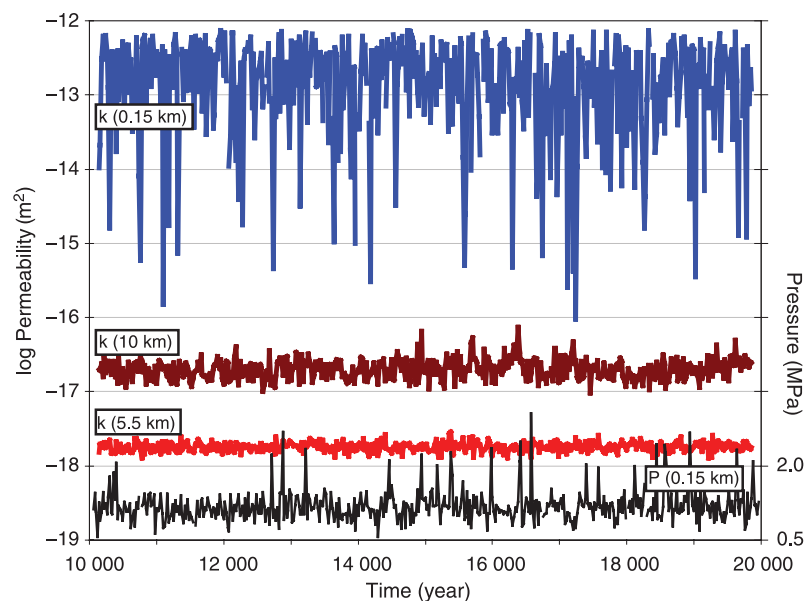

Fig. 6. Time series of pressure and permeability at selected depths along a vertical profile near the center of the model (4.5 km from the left boundary in Fig. 5). Figures 7–9 focus on mean results from simulated times of 10,000–20,000 years. The particular result shown here is for a simulation with isotropic permeability (Fig. 7). Note that in this case and at this location ($x = 4.5$ km) permeability does not decrease systematically with depth; this simulation results in a low-permeability 'wedge' that extends from the right-hand boundary to near the middle of the section (Fig. 7, inset). When we introduce a modest preference for vertical flow (Fig. 8, $k_x = 0.1k_z$), the low-permeability wedge disappears, and permeability does decrease systematically with depth throughout the model.

evolves dynamically, increasing rapidly when fluid pressure exceeds a threshold value and otherwise decaying with time towards the prescribed lower limit (10^{-19} m^2). The variations in permeability are periodic, with amplitude and frequency highly sensitive to the fluid-pressure threshold for failure, the prescribed magnitude of the associated permeability increase, and the subsequent rate of permeability loss (healing). The simulations generate permeability 'waves' that are analogous to the porosity waves described by Connolly (1997), who showed that metamorphic dehydration can lead to upward propagating dilatency waves that leave connected pore networks in their wake.

Simulations initialized with arbitrary (e.g. homogeneous) permeability distributions show irregular early-time fluctuations in permeability that are influenced by initial conditions. However, within a few thousand years permeabilities begin to oscillate fairly regularly about long-term mean values (Fig. 6). The amplitude of permeability oscillation in the simulations shows significant spatial variability but averages less than one order of magnitude in the examples considered here (e.g. Fig. 6), comparable with the magnitude of permeability changes observed in seismically influenced shallow crust in the California Coast Ranges (Rojstaczer *et al.*, 1995; Elkhoury *et al.*, 2006). The amplitude of permeability variation varies with depth but its period does not, remaining essentially constant at approximately 10^2 years in the examples considered here. We suspect, but cannot yet confirm, that the period is governed mainly by a balance between the recharge rate and the time scale governing permeability reduction.

Both the amplitude and period of the simulated permeability oscillations depend on the *ad hoc* assumptions we make about the failure threshold and rates of perme-ability increase and decrease. However, our interest here is in the quasi-steady or mean behavior of the permeability field. The mean permeability behavior – our primary concern in this paper – is affected somewhat by our *ad hoc* assumptions, but is mainly influenced by the boundary fluxes. From this point on we will focus on the mean (time-averaged) permeability structure. We wish to compare the simulated permeabilities with observational data which themselves represent averages in both time and space. The transient behavior of these simulations and its sensitivity to key parameters will be explored in a companion paper (D.O. Hayba and S.E. Ingebritsen, unpublished observations).

RESULTS

Some of our simulations entail prescribed fluxes at both upper and lower boundaries, representing external (meteoric recharge) and internal (metamorphic and magmatic) forcing, respectively (Figs 7 and 8). These simulations represent conditions in areas of active tectonism (active orogenic belts) and prograde metamorphism. Other simulations entail prescribed fluxes at the upper boundary only (Fig. 9), and represent the inactive continental crust.

Results from simulations with both external and internal forcing show enhanced permeability throughout the crustal section relative to the lower limit of 10^{-19} m^2 (Figs 7 and 8). The meteoric fluid entering at the upper boundary as a prescribed flux stays relatively close to the upper boundary, where it affects shallow permeabilities. The basal metamorphic fluid flux entering at the lower boundary rises and converges towards the lower-elevation outlet, and affects permeabilities at depth.
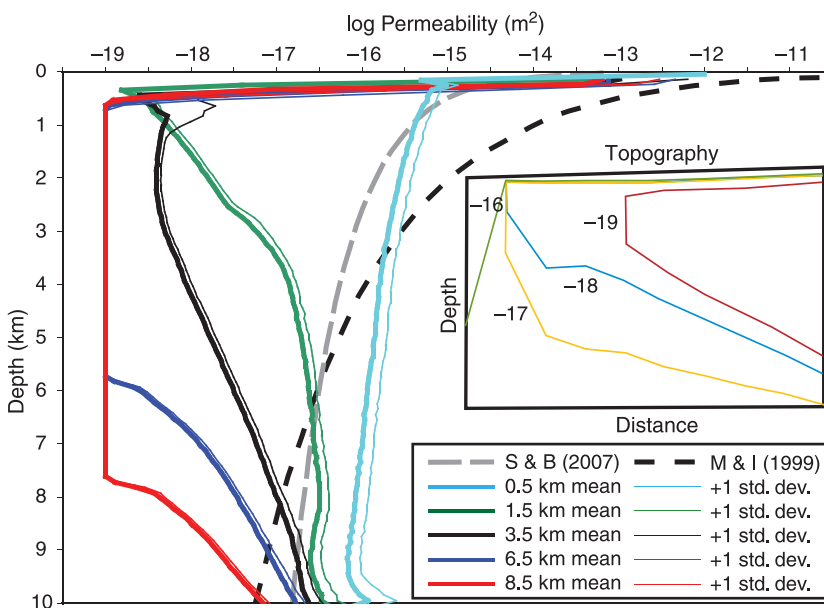

Fig. 7. Simulated permeability values in the model depicted in Fig. 5. Permeability profiles show the time-averaged, geometric mean (heavy solid lines) and geometric mean plus one standard deviation (thin solid lines) of log k along five vertical profiles at distances of 0.5, 1.5, 3.5, 6.5, and 8.5 km from the left-hand boundary (Fig. 5); permeability values were averaged at each node along the profiles for simulated times between 10,000 and 20,000 years (Fig. 6). Observationally based permeability-depth curves are shown for purposes of comparison: S&B denotes Stober and Bucher's (2007) best-fit curve from 169 well tests in the Black Forest (log k = −15.4–1.38 log z) and M&I denotes Manning and Ingebritsen's (1999) crustal-scale permeability–depth relation estimated from geothermal and metamorphic data (log k = −14–3.2 log z). Inset shows contours of mean permeability within the cross-section (Fig. 5).
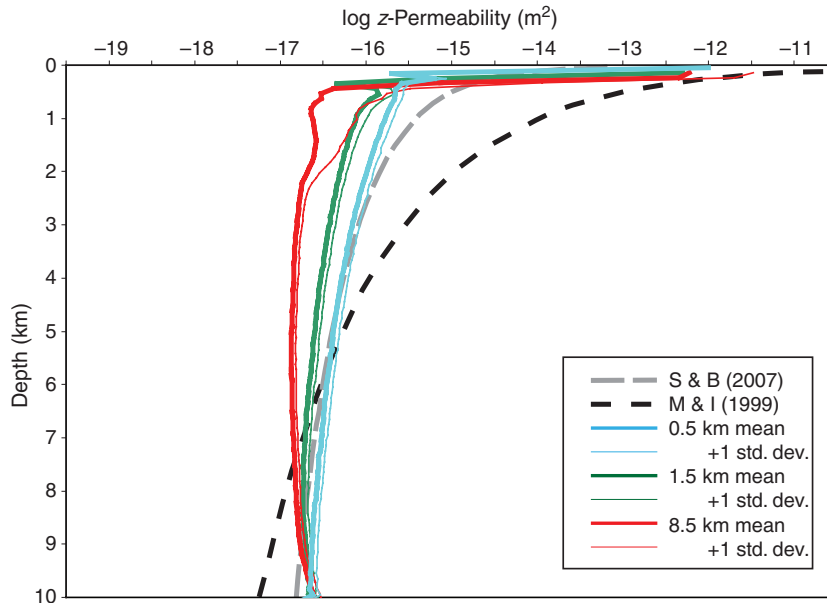
Fig. 8. Simulated permeability values in a variant of the model depicted in Fig. 5, showing the effect of a modest preference for flow in the vertical direction ($k_x = 0.1k_z$). Permeability profiles show the time-averaged, geometric mean (heavy solid lines) and geometric mean plus one standard deviation (thin solid lines) of $\log k$ at distances of 0.5, 1.5 and 8.5 km from the left-hand boundary (Fig. 5) for simulated times between 10,000 and 20,000 years. Simulated results for most of the model – between 1.5 and 8.5 km distance from the left-hand boundary – are nearly identical. Observationally based permeability–depth curves are shown for purposes of comparison: S&B denotes Stober and Bucher's (2007) best-fit curve from 169 well tests in the Black Forest ($\log k = -15.4 - 1.38 \log z$) and M&I denotes Manning and Ingebritsen's (1999) crustal-scale permeability–depth relation estimated from geothermal and metamorphic data ($\log k = -14 - 3.2 \log z$).
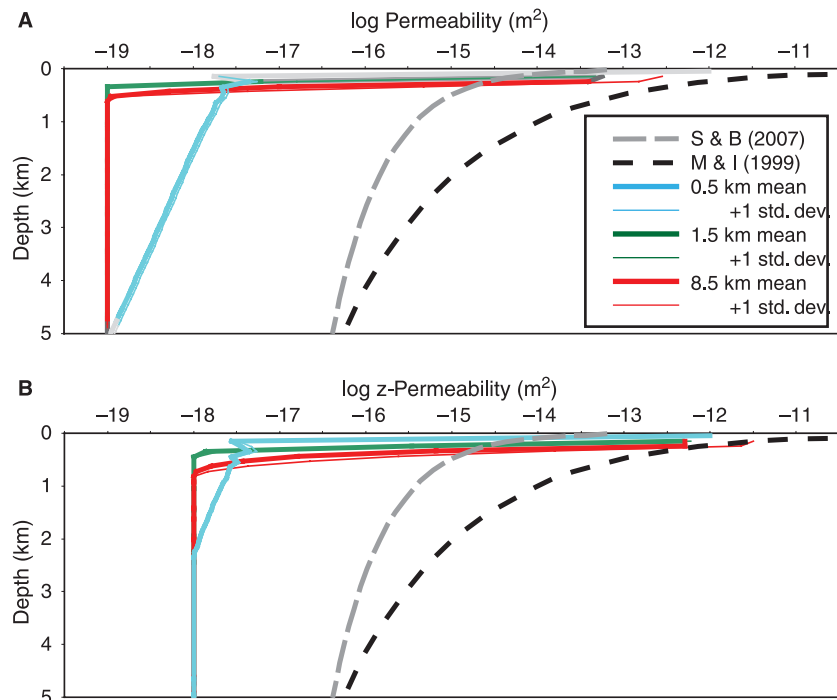

Fig. 9. Simulated permeability values from simulations with prescribed fluxes at the upper boundary only (A) for the isotropic case ($k_x = k_z$) and (B) for $k_x = 0.1\,k_z$. Permeability profiles show the time-averaged, geometric mean (heavy solid lines) and geometric mean plus one standard deviation (thin solid lines) of $\log k$ at distances of 0.5, 1.5 and 8.5 km from the left-hand boundary (Fig. 5) for simulated times between 10,000 and 20,000 years. Observationally based permeability–depth curves are shown for purposes of comparison, as described in the captions of Figures 7 and 8.

For isotropic permeabilities ($k_x = k_z$) the permeability-enhancing effects of meteoric recharge are seen only in the upper kilometer of the crust (Fig. 7). Here, permeability is very heterogeneous, with $\log k$ ranging from -19 to -12. Because both the surface flux and the basal flux converge towards the lower-elevation outlet, there is a large,

wedge-shaped region of the domain with little flow (Fig. 7, inset) and low permeabilities.

Introducing a modest preference for flow in the vertical direction ($k_x = 0.1 k_z$) – to represent the possible effect of extensional tectonics and/or vertical jointing – has a large influence on the simulated permeability regime (Fig. 8). Simulated permeability in the upper 1 kilometer of the crust remains heterogeneous but the simulated range in log k_z is reduced substantially (compare Figs 7 and 8). The permeability-enhancing effect of meteoric recharge extends deeper but still does not extend below about 1 km. The most dramatic effect of invoking $k_x = 0.1 k_z$ is seen at greater depths, where mean log k_z now lies between −17 and −16 and is relatively uniform in space and time. Because of the preference for vertical flow, the basal metamorphic fluid flux no longer converges towards the lower-elevation outlet, and instead rises uniformly through the section. This modest anisotropy causes the permeability of the lower part of the section to be relatively high and uniform. Introducing greater anisotropy ($k_x = 0.01 k_z$) does not significantly change the permeability distribution.

Figures 7 and 8 compare the simulated permeabilities with permeability-depth relations based on observational data from the Black Forest (log $k = -15.4 - 1.38 \log z$; Stober and Bucher, 2007) and with the global compilation of geothermal and metamorphic data (log $k = -14 - 3.2 \log z$; Manning and Ingebritsen, 1999). Below about 2 km depth, mean simulated permeabilities in Fig. 8 track the Stober and Bucher (2007) curve particularly well.

Results from simulations with prescribed fluxes at the upper boundary only, representing the inactive continental crust, are depicted in Fig. 9. In the absence of a basal fluid flux, permeability generally decays towards the prescribed lower limit within the upper 0.5 km of the section. Enhanced permeability persists to greater depths near the lower-elevation outlet: to roughly 5 km depth in the isotropic case (Fig. 9A) and to roughly 2 km depth when we introduce a modest preference for flow in the vertical direction ($k_x = 0.1 k_z$, Fig. 9B).

We can compare the mean permeability of the uppermost crust from our simulations with the value of log $k = -14$ derived both from *in situ* well-test data (Brace, 1980) and our first-order, recharge-based calculations (Fig. 4). In the simulations depicted in Figures 7–9, the arithmetic mean permeability ranges from log $k_x = -15.7$ to −15.1 when evaluated between 0 and 0.5 km depth and from log $k_x = -16.3$ to −17.4 when evaluated between 0 and 1.0 km depth. Because of the strong depth dependence of simulated permeability in the upper kilometer of the crust (Figs 7–9), the mean value is highly dependent on the depth interval over which it is evaluated. The mean value evaluated over the upper few hundred meters of the section would be similar to the values obtained from well-test data and recharge-based calculations. Regardless

of the depth interval considered, the simulations show mean log k of the uppermost crust to be only weakly sensitive to the presence (Figs 7 and 8) or absence (Fig. 9) of a small prescribed flux at the lower boundary, despite the controlling influence of the lower-boundary flux on permeabilities deeper in the section.

DISCUSSION

Simulations with both internal and external forcing show enhanced permeability throughout the model domain, relative to the prescribed lower limit of 1×10^{-19} m^2 (Figs 7 and 8). The presence of a wedge-shaped region of low permeability when $k_x = k_z$ (Fig. 7, inset) and its absence when $k_x < k_z$ (Fig. 8) suggests the possibility of a systematic difference in the gross permeability structure between regions of compressional and extensional tectonics. Simulations with only external forcing show enhanced permeability confined to roughly the upper 0.5 km of the section (Fig. 9), except near the lower-elevation outlet.

The internal forcing represents a deep fluid flux typical of regions of Neogene tectonism, magmatism, and metamorphism, which occupy roughly 10% of the area of the continental crust (Barnes et al., 1984). First-order calculations assuming a near-lithostatic fluid-pressure gradient show that mean permeabilities of 10^{-20} to 10^{-18} m^2 are required to accommodate typical metamorphic devolatilization fluxes in the range of 10^{-12}–10^{-11} m s^{-1} (e.g. Manning and Ingebritsen, 1999). The somewhat larger mean permeabilities required in our simulations – 10^{-17} m^2 or more in Figure 8 – reflect the near-hydrostatic pressure conditions and higher fluid viscosities in the simulations. The generally convex-upward shape of the simulated permeability–depth relations below 2–3 km depth (e.g. Fig. 8) results from the increasing viscosity of the rising, cooling fluid. Fluid viscosity increases roughly 16-fold between the base of the model and the low-elevation discharge area.

Simulations with external forcing only (Fig. 9) are presumably more representative of conditions in the inactive crust and show significantly different permeability–depth relations relative to the active crust (Figs 7–8). Permeability may decrease more rapidly with depth where internal (metamorphic and magmatic) forcing is insignificant. In fact, there are strong petrologic arguments for a 'dry', very-low-permeability crust in regions of retrograde metamorphism. In such regions no free, connected fluid phase can persist at depth, because infiltration of fluid in the cooling (or substantially cooled) rock will result in hydration reactions that decrease permeability (e.g. Yardley and Valley, 1997; Yardley and Baumgartner, 2007). Water-consuming reactions in cooling crystalline rocks may actually generate subhydrostatic fluid pressures and promote a continuous flow of fluid to the deeper parts of the upper crust (e.g. Yakovlev, 1993; Stober and Bucher, 2004).

Comparison of simulation results with (Figs 7–8) and without (Fig. 9) a basal metamorphic fluid flux provides some insight on a point that has interested us for some time: the physical implications of the empirical constants in the curve fit to geothermal and metamorphic data (log $k = -14 - 3.2\log z$, where z is depth in kilometers) (Manning and Ingebritsen, 1999). The constant -14 is consistent with the mean permeability of the uppermost crust, as defined independently both by *in situ* well-test data (Brace, 1980) and the first-order, recharge-based calculations reported here (Fig. 4). The coefficient -3.2 reflects the magnitude of deep metamorphic (or other endogeneous) fluid fluxes. Its magnitude should be inversely related to the magnitude of any deep fluid source.

Our simulations suggest that, regardless of whether the lower crust is active or inactive, the permeability of the shallow, crystalline crust will exhibit substantial temporal and spatial heterogeneity (Figs 6–9). However, the mean, large-scale permeability of the uppermost crust should cycle about an 'optimum' level that that is tuned to both the state of stress and the rate of groundwater recharge. It is likely governed by a network of interconnected, critically stressed fractures. Without episodic failure, mineral precipitation and alteration will tend to seal fractures over time, reducing permeability. Given a constant rate of recharge, water-table elevation (fluid pressures) will then rise, decreasing the effective stress, reinitiating slip on fractures, and enhancing permeability. Similarly, an increased rate of recharge should increase water-table elevation (fluid pressures) and initiate slip, enhancing permeability. In either event there should be a tendency for mean permeability to vary about an optimal level determined by the state of stress and the recharge rate.

Permeability should also be expected to respond to temporal variability in the Earth's climate. Climate variability on time scales ranging up to glacial–interglacial will certainly influence the magnitude of external forcing and could conceivably affect internal forcing as well (e.g. McPherson and Bredehoeft, 2001). The influence of reservoir filling on effective stress and seismicity is well documented (cf. Talwani *et al.*, 2007). Water-table variations over geologic time scales could cause similar or even larger variations in effective stress. Hydrogeologists expect the water table to mimic topography (Fig. 2), but not to coincide with it, except where there is localized groundwater discharge. Depth to water table from the land surface depends mainly on recharge rate and permeability (Forster and Smith, 1989) and ranges from a few meters to approximately 500 m, with the largest excursions from the land surface occurring in regions of moderate to great topographic relief, high permeability, and/or arid climates (e.g. Kilauea volcano, Hawaii; the High Lava Plains of Oregon; and the Basin and Range province of the western United States). Thus an increase in recharge can potentially increase water-table elevation (and subsurface fluid pressures) by meters to hundreds of meters (up to approximately 5 MPa) and thereby decrease the effective stress, potentially initiating slip on fractures and enhancing permeability. Because of the slowness of pressure diffusion in low-permeability media, there is the potential for large lag times between changes in forcing and full pressure equilibration in regional groundwater flow systems (for instance, offshore freshwater widely observed at mid-latitudes may still reflect Pleistocene sea levels: Essaid, 1990; Kooi *et al.*, 2000; Person *et al.*, 2003).

Our conceptual model implies that spatial variability in the external and internal forcings should cause significant geographic variability in permeability–depth relations. Here, however, we have conditioned our calculations on average conditions in the western United States. This approach lumps a wide range of recharge rates and 'active' and 'inactive' crust. Our conceptual model implies, for instance, differences in the deep permeability structure between the Sierra Nevada (high relief, high recharge) and southern Arizona (lower relief, low recharge), or between the California Coast Ranges (active metamorphism) and the Rockies (little or no active metamorphism). Unfortunately, current data do not permit meaningful comparison among geographic regions. Deep, *in situ* permeability data represent isolated pinpricks in the Earth's upper crust. They scarcely suffice for global inferences about permeability–depth relations (e.g. Manning and Ingebritsen, 1999; Townend and Zoback, 2000) and do not yet permit comparison among geographic regions.

ACKNOWLEDGEMENTS

REFERENCES

Barnes I (1970) Metamorphic waters from the Pacific tectonic belt of the United States. *Science*, **168**, 973–5.

Barnes I, Irwin WP, White DE (1984) Map showing world distribution of carbon-dioxide springs and major zones of seismicity. U.S. Geological Survey Miscellaneous Investigations Map I-1528, scale 1:40,000,000.

Barton CA, Zoback MD, Moos D (1995) Fluid flow along potentially active faults in crystalline rock. *Geology*, **23**, 683–6.

Bettinelli P, Avouac J-P, Flouzat M, Bollinger L, Ramillien G, Raj-aure S, Sapkota S (2008) Seasonal variations of seismicity and geodetic strain in the Himalaya induced by surface hydrology. *Earth and Planetary Science Letters*, **266**, 332–44.

Bollinger L, Perrier F, Avouac J-P, Sapkota S, Gautam U, Tiwari DR (2007) Seasonal modulation of seismicity in the Himalaya of Nepal. *Geophysical Research Letters* **34**, L08304, doi:10.1029/2006GL029192.

Brace WF (1980) Permeability of crystalline and argillaceous rocks. *International Journal of Rock Mechanics and Mining Sciences and Geomechanics Abstracts*, **17**, 241–51.

Cathles LM, Adams JJ (2005) Fluid flow and petroleum and mineral resources in the upper (<20 km) continental crust. *Economic Geology*, 100th Anniversary Volume, 77–110.

Christiansen LB, Hurwitz S, Ingebritsen SE (2007) Annual modulation of seismicity along the San Andreas Fault near Parkfield, CA. *Geophysical Research Letters*, **34**, L04306, doi:10.1029/2006GL028634.

Christiansen LB, Hurwitz S, Saar MO, Ingebritsen SE, Hsieh PA (2005) Seasonal seismicity at western United States volcanoes. *Earth and Planetary Science Letters*, **240**, 307–21.

Claesson L (2007) *Fluid-rock interaction in two seismically active areas*. PhD thesis, Stockholm University, Sweden, 70 p. + appendices.

Claesson L, Skelton A, Graham C, Morth CM (2007) The time-scale and mechanisms of fault sealing and water-rock interaction after an earthquake. *Geofluids*, **7**, 427–40.

Clauser C (1992) Permeability of crystalline rocks. *Eos, Transactions of the American Geophysical Union*, **73**, 233–37.

Connolly JAD (1997) Devolatilization-generated fluid pressure and deformation-propagated fluid flow during prograde regional metamorphism. *Journal of Geophysical Research*, **102**, 18,149–73.

Crossey LJ, Fischer TP, Patchett PJ, Karlstrom KE, Hilton DR, Newell DL, Huntoon P, Reynolds AC, de Leeuw GAM (2006) Dissected hydrologic system at the Grand Canyon: interaction between deeply derived fluids and plateau aquifer waters in modern springs and travertine. *Geology*, **34**, 25–8.

Dahlgren S, Bogoch R, Magaritz M, Michard A (1993) Hydro-thermal dolomite marbles associated with charnockitic magmatism in the Proterozoic Bramble Shear Belt, south Norway. *Contributions to Mineralogy and Petrology*, **113**, 394–409.

Dunai TJ, Touret JLR (1993) A noble gas study of a granulite sample from the Nilgiri Hills, southern India: implications for granulite formation. *Earth and Planetary Science Letters*, **119**, 271–81.

Elkhoury JE, Brodsky EE, Agnew DC (2006) Seismic waves increase permeability. *Nature*, **441**, 1135–8.

Essaid HI (1990) A multilayered sharp interface model of coupled freshwater and saltwater flow in coastal systems: model development and application. *Water Resources Research*, **26**, 1431–54.

Evans KF, Genter A, Sausse J (2005) Permeability creation and damage due to massive fluid injections into granite at 3.5 km at Soultz: 1. Borehole observations. *Journal of Geophysical Research*, **110**, B04203, doi:10.1029/2004JB003168.

Faust CR, Mercer JW (1979a) Geothermal reservoir simulation. 1. Mathematical models for liquid- and vapor-dominated hydro-thermal systems. *Water Resources Research*, **15**, 23–30.

Flint AL, Flint LE, Kwicklis EM, Fabryka-Martin JT, Bodvars-son GS (2002) Estimating recharge at Yucca Mountain, Nevada: comparison of methods. *Hydrogeology Journal*, **10**, 180–204.

Forster C, Smith L (1989) The influence of groundwater flow on thermal regimes in mountainous terrain: a model study. *Journal of Geophysical Research*, **97**, 9439–51.

Fyfe WS, Price NJ, Thompson AB (1978) *Fluids in the Earth's Crust*. Elsevier Scientific, New York.

Hainzl S, Kraft T, Wasserman J, Ingel H, Schmedes E (2006) Evidence for rainfall triggered earthquake activity. *Geophysical Research Letters*, **33**, L19303, doi:10.1029/2006GL027642.

Hanson RB (1992) Effects of fluid production on fluid flow during regional and contact metamorphism. *Journal of Metamorphic Geology*, **10**, 87–97.

Hanson RB (1995) The hydrodynamics of contact metamorphism. *Geological Society of America Bulletin*, **107**, 595–611.

Hanson RB (1997) Hydrodynamics of regional metamorphism due to continental collision. *Economic Geology*, **92**, 880–91.

Hayba DO, Ingebritsen SE (1994) The computer model HYDROTHERM, a three-dimensional finite-difference model to simulate ground-water flow and heat transport in the temperature range of 0 to 1,200°C. U.S. Geological Survey Water-Resources Investigations Report, 94–4045.

Heki K (2003) Snow load and seasonal variation of earthquake occurrence in Japan. *Earth and Planetary Science Letters*, **207**, 159–64.

Hsieh PA (1998) Scale effects in fluid flow through fractured geologic media. In: *Scale Dependence and Scale Invariance in Hydrology* (ed. Sposito G), pp. 335–53. Cambridge University Press, New York.

Hsieh PA, Bredehoeft JD (1981) A reservoir analysis of the Denver earthquakes: a case of induced seismicity. *Journal of Geophysical Research*, **86**, 903–20.

Huenges E, Erzinger J, Kuck J, Engeser B, Kessels W (1997) The permeable crust: geohydraulic properties down to 9101 m depth. *Journal of Geophysical Research*, **102**, 18,255–65.

Ingebritsen SE, Manning CE (1999) Geological implications of a permeability-depth curve for the continental crust. *Geology*, **27**, 1107–10.

Ingebritsen SE, Manning CE (2002) Diffuse fluid flux through orogenic belts: implications for the world ocean. *Proceedings of the National Academy of Sciences USA*, **99**, 9113–6.

Ingebritsen SE, Sanford WE, Neuzil CE (2006) *Groundwater in Geologic Processes*, 2nd edn. Cambridge University Press, Cambridge.

Ingebritsen SE, Scholl MA (1993) The hydrogeology of Kilauea volcano. *Geothermics*, **22**, 255–70.

James ER, Manga M, Rose TP (1999) CO_2 degassing in the Oregon Cascades. *Geology*, **27**, 823–6.

Kamensky IL, Tolstikhin IN, Vetrin VR (1990) Juvenile helium in ancient rocks: I. ^{3}He excess in amphiboles from 2.8-Ga charnockite series – crust-mantle fluid in intracrustal magmatic processes. *Geochimica et Cosmochimica Acta*, **54**, 3115–22.

Kennedy BM, van Soest MC (2007) Flow of mantle fluids through a ductile lower crust: helium isotope trends. *Science*, **318**, 1433–6.

Kooi H, Groen J, Leijnse A (2000) Modes of seawater intrusion during transgressions. *Water Resources Research*, **36**, 3581–9.

Lowell RP, Van Cappellen P, Germanovich LN (1993) Silica precipitation in fractures and the evolution of permeability in hydrothermal upflow zones. *Science*, **260**, 192–4.

Manning CE, Ingebritsen SE (1999) Permeability of the continental crust: the implications of geothermal data and metamorphic systems. *Reviews of Geophysics*, **37**, 127–50.

Marder M, Fineberg J (1996) How things break. *Physics Today*, **49**(9), 24–9.

McPherson BJOL, Bredehoeft JD (2001) Overpressures in the Uinta basin, Utah: analysis using a three-dimensional basin evolution model. *Water Resources Research*, **37**, 857–71.

Mitchell JK (1993) *Fundamentals of Soil Behavior*, 2nd edn. John Wiley and Sons, New York.

Moglen GE, Eltahir EAB, Bras RL (1998) On the sensitivity of drainage density to climate change. *Water Resources Research*, **34**, 855–62.

Moore DE, Morrow CA, Byerlee JD (1983) Chemical reactions accompanying fluid flow through granite held in a temperature gradient. *Geochimica et Cosmochimica Acta*, **47**, 445–53.

Newell DL, Crossey LJ, Karlstrom KE, Fischer TP, Hilton DR (2005) Continental-scale links between the mantle and groundwater systems of the western United States: evidence from travertine springs and regional He data. *GSA Today*, **15**(12), 4–10.

Ohtake M, Nakahara H (1999) Seasonality of great earthquake occurrence at the northwestern margin of the Philippine Sea plate. *Pure and Applied Geophysics*, **155**, 689–700.

Oliver NHS, Cartwright I, Wall VJ, Golding DS (1993) The stable isotope signature of kilometre-scale fracture-dominated metamorphic fluid pathways, Mary Kathleen, Australia. *Journal of Metamorphic Geology*, **11**, 705–20.

Person MA, Dugan B, Swenson JB, Urbano L, Stott C, Taylor J, Millet M (2003) Pleistocene hydrogeology of the Atlantic continental shelf, New England. *Geological Society of America Bulletin*, **115**, 1324–43.

Rodriguez-Iturbe I, Rinaldo A (1997) *Fractal River Basins: Chance and Self-Organization*. Cambridge University Press, Cambridge.

Rojstaczer SA, Bredehoeft JD (1988) Groundwater and fault strength. In: *The Geology of North America v. O-2: Hydrogeology* (eds Back W, Rosenshein JS, Seaber PR), pp. 447–60. The Geological Society of America, Boulder, CO.

Rojstaczer SA, Wolf S, Michel R (1995) Permeability enhancement in the shallow crust as a cause of earthquake-induced hydrological changes. *Nature*, **373**, 237–9.

Saar MO, Manga M (2003) Seismicity induced by seasonal groundwater recharge at Mt. Hood, Oregon. *Earth and Planetary Science Letters*, **214**, 605–18.

Saar MO, Manga M (2004) Depth dependence of permeability in the Oregon Cascades inferred from hydrogeologic, thermal, seismic, and magmatic modeling constraints. *Journal of Geophysical Research*, **109**, B04204, doi:10.1029/2003JB002855.

Scholz CH (2002) *The Mechanics of Earthquakes and Faulting*, 2nd edn. Cambridge University Press, Cambridge.

Sclater JG, Jaupart C, Galson D (1980) The heat flow through oceanic and continental crust and the heat loss of the Earth. *Reviews of Geophysics and Space Physics*, **18**, 269–311.

Shmonov VM, Vitiovtova VM, Zharikov AV, Grafchikov AA (2003) Permeability of the continental crust: implications of experimental data. *Journal of Geochemical Exploration*, **78/79**, 697–9.

Sibson RH (1996) Structural permeability of fluid-driven fault-fracture meshes. *Journal of Structural Geology*, **18**, 1031–42.

Stober I, Bucher K (2004) Fluid sinks within the Earth's crust. *Geofluids*, **4**, 143–51.

Stober I, Bucher K (2007) Hydraulic properties of the crystalline basement. *Hydrogeology Journal*, **15**, 213–24.

Talwani P, Chen L, Gahalaut K (2007) Seismogenic permeability, k_s. *Journal of Geophysical Research*, **112**, B07309, doi:10.1029/2006JB004665.

Toth J (1963) A theoretical analysis of groundwater flow in small drainage basins. *Journal of Geophysical Research*, **68**, 4795–812.

Townend J, Zoback MD (2000) How faulting keeps the crust strong. *Geology*, **28**, 399–402.

Winograd IJ (1971) Hydrogeology of ash-flow tuff: a preliminary statement. *Water Resources Research*, 7, 994–1006.

Wolf LW, Rowe CA, Horner RB (1997) Periodic seismicity on the Alaska-British Columbia border: a case for hydrologically triggered earthquakes. *Bulletin of the Seismological Society of America*, **87**, 1473–83.

Wolock DM, McCabe GJ (2000) Differences in topographic characteristics computed from 100- and 1000-m resolution digital elevation model data. *Hydrological Processes*, **14**, 987–1002.

Yakovlev LYe (1993) The role of metamorphism of the basaltic basement of sedimentary basins in crustal evolution. *International Geology Review*, **35**, 27–47.

Yardley BWD (1986) Fluid migration and veining in the Connemara Schists, Ireland. In: *Fluid-Rock Interactions During Metamorphism* (eds Walther JV, Woods BJ), pp. 109–31. Springer-Verlag, New York.

Yardley BWD, Baumgartner LP (2007) Fluid processes in deep crustal fault zones. In: *Tectonic Faults − Agents of Change on a Dynamic Earth* (eds Handy MR, Hirth G, Hovius N), pp. 295–318. The MIT Press, Cambridge, MA.

Yardley BWD, Valley JW (1997) The petrologic case for a dry lower crust. *Journal of Geophysical Research*, **102**, 12,173–85.

Zoback ML, Zoback MD (1997) Crustal stress and intraplate deformation. *Geowissenschaften*, **15**, 116–23.